PCCP

Accepted Manuscript

ROYAL SOCIETY OF CHEMISTRY

www.rsc.org/pccp

Physical Chemistry Chemical Physics
CREATED USING THE RSC LaTeX PCCP ARTICLE TEMPLATE – SEE www.rsc.org/electronicfiles FOR DETAILS
ARTICLE TYPE
www. rsc.org/xxxxxx | XXXXXXXX

Structural and electronic properties of Pt_n/PAH complex (n=1, 2) from density functional calculations

Mehdi Mahmoodinia[a], Mahsa Ebadi[a], Per-Olof Åstrand[a,*], De Chen[b], Hong-Ye Cheng[c], and Yi-An Zhu[c]

Received Xth XXXXXXXXXX 20XX, Accepted Xth XXXXXXXXX 20XX
First published on the web Xth XXXXXXXXXX 200X
DOI: 10.1039/b000000x

A detailed density functional study of the Pt atom and Pt dimer adsorption on a polyaromatic hydrocarbon (PAH) is presented. The preferred adsorption site for a Pt atom is confirmed to be the bridge site. Upon adsorption of a single Pt atom, however, it is found here that the electronic ground state changes from the triplet state ($5d^9 6s^1$ configuration) to the closed-shell singlet state ($5d^{10}6s^0$ configuration), which consequently will affect the catalytic activity of Pt when single Pt atoms bind to a carbon surface. The preferred adsorption site for the Pt dimer in the upright configuration is the hollow site. In contrast to the adsorption of a single Pt atom, the formation of a Pt-C bond in the adsorption of a Pt dimer is not accompanied by a change in the spin state, so the most stable electronic state is still the triplet state. While the atomic charge on the Pt atoms and dimers (in parallel configuration) in the Pt_n/PAH complex is positive, a negative charge is found on the upper Pt atom for the upright configuration, indicating that single layers of Pt atoms will have a different catalytic activity as compared to Pt clusters on a carbon surface. Comparing the Pt-C bond length and the charge transfer on different sites, the magnitude of the charge transfer decreases with bond elongation, indicating that the catalytic activity of the Pt atom and dimer can be changed by modifying its chemical surroundings. The adsorption energy for the Pt dimer on a PAH surface is larger than for two individual Pt atoms on the surface indicating that aggregation of Pt atoms on the PAH surface is favorable.

1 Introduction

Graphene is a two-dimensional honeycomb lattice[1–3] which among carbon materials has attracted great attention due to its fascinating properties including high surface area[4], linear dispersion of electronic states at the Fermi level[5], a semiconductor with zero bandgap[6], superior electric conductivity[7], excellent mechanical strength[8] and high thermal stability[7]. There has also been focus on adsorption of metal clusters on graphene[9–15]. For example, adsorption of different metal adatoms on graphene has been studied[10], electronic and magnetic properties of graphene functionalized by 3*d* transition-metal atoms have been investigated[12], and electronic structures and magnetic properties of transition metal M (Fe, Co, Ni, and Cu) adatom and dimer adsorbed on graphene have been studied[11].

Platinum nanoparticles occupy a privileged position as a catalyst in industrial applications[16]. In direct methanol fuel cells (DMFC) and proton exchange membrane fuel cells (PEMFC), Pt nanoparticles supported on carbon materials are used as an electrode catalyst for both hydrogen oxidation at the anode and oxygen reduction at the cathode[17,18]. The ultimate goal is to control the size and shape of the metallic particle to promote the catalytic activity, and thereby reduce costs and prolong device lifetimes[19–25]. To improve catalytic activity, graphene may play an important role by stabilizing the metal nanoparticles on the surface. In this regard, it is necessary to understand the microstructure of Pt/C to analyze the interaction between the Pt atoms and the carbon surface, and

[a] *Department of Chemistry, Norwegian University of Science and Technology, 7491 Trondheim, Norway*
[b] *Department of Chemical Engineering, Norwegian University of Science and Technology (NTNU), 7491 Trondheim, Norway*
[c] *State Key Laboratory of Chemical Engineering, East China University of Science and Technology (ECUST), Shanghai 200237, China*
∗ *Corresponding author.*
E-mail address: per-olof.aastrand@ntnu.no (P.-O. Åstrand).

to investigate the stability of Pt nano-particles on carbon materials.

There are several theoretical efforts devoted to an improved understanding of the Pt-C interaction[10–15,26–37]. Kong et al., investigated the single Pt-atom adsorption on a carbon nanotubes (CNTs) and graphite nano-fibers (GNFs)[27], and observed strong adsorption on atomic vacant sites or graphene edges. Okazaki-Maeda and co-workers examined the interactions of a small Pt clusters and a Pt(111) surface with a graphene sheet using density functional calculations[15,29,30]. They found that the interaction between the Pt cluster and the graphene surface strongly depends on the shape and size of a cluster. On the experimental side, scanning tunneling microscopy (STM) and X-ray photoelectron spectroscopy (XPS) have been used to investigate the small Pt clusters on the basal plane of highly oriented pyrolytic graphite (HOPG)[38,39]. The average bond length of a Pt-dimer and trimers on graphite is predicted to be 2.45 and 2.66 Å, respectively. Howells and co-workers[40] investigated the influence of substrate defect sites on the morphology of Pt vapor deposited on the basal plane of HOPG by XPS and STM and indicated that the interaction between a Pt cluster and HOPG depends on the surface condition of HOPG.

Density functional theory (DFT) has become an invaluable tool in studying the interaction between metal clusters and graphene at the atomic level[9–15]. However, when considering this type of interaction, the effect of dispersion forces becomes important, as for example in the adsorption of aromatic molecules on metal surfaces[41–47]. The standard generalized gradient approximation (GGA) functionals, such as the Perdew-Burke-Ernzerhof (PBE)[48] functional, do not describe this effect, since it cannot describe electron correlation in situations where the electronic densities of the molecule and surface in practice do not overlap and the dispersion interaction become dominant[41,49]. Grimme's dispersion correction[50,51] has been demonstrated to successfully stabilize the adhesion of a graphene layer on a Ni(111) substrate[52] and adsorption of Pt atom on graphene surface[47]. The Swart-Solá-Bickelhaupt (SSB-D) functional[53,54], was constructed on the basis of a small correction of the PBE functional, together with Grimme's dispersion correction and it was shown to work well for spin states of transition metal complexes, S_N2 reaction barriers, accuracy of geometries, hydrogen bonding, and $\pi - \pi$ stacking interactions.

One of the most important factors for a correct description of heavy transition metals such as Pt is undoubtedly relativistic effects[55–58]. An accurate way to include relativistic effects is to use the full four-component Dirac equation[59], however the application of such approaches is still considerably time-consuming and not suitable for applications like the interaction between Pt clusters and carbon surfaces. To avoid this complexity various approximate quasi-relativistic approaches have been proposed, such as one- or two-component approximate relativistic models, like the Douglas-Kroll transformation[60–62], and the zero-order-regular approximation (ZORA) equation[63–68], where the ZORA Hamiltonian gives accurate results especially for valence orbitals[65]. Therefore all-electron calculations for chemical systems containing heavy elements are critically depends on the level of quantum chemical theory and on the way relativistic effects are treated[69]. The ZORA full electron approach with large basis set like QZ4P put limitation on in particular the number of heavy elements including in our systems. A successful route is also to use relativistic effective core potentials (pseudopotentials)[70–72], where the relativistic effects are included in the effective potential, to study the relativistic effects for systems containing large numbers of heavy elements[14,15,30].

Polyaromatic hydrocarbons (PAH) have been demonstrated as a good substrate to stabilize the single Pt[47] and Co[73] atoms and considered as model structures for the adsorption of Pt dimers on graphene. Also, graphene is an ideal system whereas real systems include defects, therefore bonding to PAHs represents a model for binding to the π system relatively near defects in a real graphene material. Most of these studies[10–15,26–37] have concentrated on the structural and energetic properties of the adsorbate-graphene system, and there are only a few results about charge transfer in the Pt/C system[47]. Also the spin multiplicity (or spin state) of the Pt/C system needs to be studied in more detail[74].

Therefore, we investigate here the stability of the Pt atom and dimer on a PAH model at several different adsorption sites and for different spin states. We also analyze adsorption energies, interfacial interaction energies, Pt-C distances, Pt-Pt distances, and Pt-PAH charge transfer in terms of atomic charges. Furthermore, to elucidate the

nature of the interaction, we visualize the molecular orbitals to provide further insight into the nature of these interactions.

2 Computational details

All calculations are based on DFT as implemented in the Amsterdam Density Functional (ADF) package[75,76]. The molecular orbitals (MOs) were expanded in an uncontracted set of Slater-type orbitals (STO), the QZ4P basis set[77], based on a previous basis set study[47]. Slater-type functions are substantially more diffuse than a corresponding Gaussian basis set and give consistent and rapidly converging results, while the convergence with respect to basis set size is much slower for Gaussian type basis sets. This may be related to the cusp at the nuclei that is correctly described by STOs[78]. The QZ4P basis set has triple-quality in the core and quadruple-quality in the valence orbitals, and it is also augmented by four sets of polarization functions which is included mostly for a better description of molecular properties. Since some orbitals become almost linearly dependent, a few orbitals are removed during the calculation.

The ZORA kinetic energy can be split into a scalar relativistic part and a spin-orbit coupling term, but since a single Pt atom and dimer in any of the adsorption sites of graphene, expect in upright configurations, do not possess a magnetic moment[33], only scalar relativistic effects without spin-orbit coupling are considered in this work.

In this work a $C_{40}H_{16}$ molecule is chosen as a PAH model system as a representative example. Several PAH models were investigated in Ref.[47] and indeed it was found that the result depend significantly on the choice of a PAH model. We believe, however, that the type of system studied here is more realistic (since we always have defects and impurities) than a perfect graphene plane.

Several spin states for the Pt_n/PAH (n=1, 2) complex are studied with the SSB-D functional, which has been demonstrated to be successful for describing spin states of transition-metal complexes[54,79]. Many standard density functionals fail to predict the spin ground-state of transition-metal complexes[80] and the SSB-D functional was specifically designed to do well in this respect[54]. The spin state is denoted with the spin multiplicity $2S+1$, which is 1 for a singlet state, 3 for a triplet state and 5 for a quintet state. The energies are calculated using both spin-restricted and spin-unrestricted methods. Two types of energies are used to analyze the stability of the adsorbed system and the Pt_n/PAH interactions. The adsorption energy, E_{ads}, is defined as

$$E_{ads} = E_{Pt_n/PAH} - E_{PAH} - nE_{Pt} \quad (1)$$

where $E_{Pt_n/PAH}$, E_{PAH} and E_{Pt} are the energies of the Pt_n/PAH system, the PAH molecule and an isolated Pt atom, respectively. Also the interfacial interaction energy, E_{int}, defined as

$$E_{int} = E_{Pt_2/PAH} - E_{PAH} - E_{Pt_2} \quad (2)$$

is calculated, where E_{Pt_2} is the binding energy of a Pt dimer in the gas phase. The interfacial interaction energy measures the interaction energy of Pt dimer with the PAH surface, and consists of a negative contribution from the energy gained by forming Pt_2-PAH bonds and positive contributions from the distortions of both the Pt dimer and the PAH molecule. In addition, we examined the binding energy, E_b, of the Pt dimer in gas phase

$$E_b = E_{Pt_2} - 2E_{Pt}. \quad (3)$$

The atomic charges are obtained by Hirshfeld charges[81,82] which are evaluated by numerical integration in ADF, and appear to be reliable and not very sensitive to basis set effects[75]. In geometry optimization of non-stable configurations, we have imposed constraints in the x and y coordinates of Pt atom and dimer to keep them in the expected binding site. We visualize the MOs by using the ADF graphical user interface and the VESTA program[83].

3 Results and Discussion

This section consists of four parts. First, we study briefly the electronic structure of the Pt atom and dimer in the gas phase. Secondly, we investigate the PAH system. In the next step, the adsorption energies as well as electronic and geometric properties of the Pt/PAH complex at different adsorption sites are presented and discussed. Finally, we analyze the same characteristics for the Pt_2/PAH complex.

3.1 Platinum atom and dimer in the gas phase

Before going further into the study of the structure of Pt_n/PAH complexes, it is useful to evaluate briefly the electronic structure of the Pt atom and dimer since their characteristics have major influence on the properties of the Pt_n/PAH complex and also these characteristics may change after adsorption on the PAH surface.

For the Pt atom, the triplet state ($5d^9 6s^1$ configuration) is the electronic ground state[84], which is confirmed by the SSB-D functional in Table 1. The singlet ($5d^{10}6s^0$configuration) and quintet ($5d^8 6s^1 6p^1$configuration) states are 0.12 and 5.40 eV higher in energy, respectively. For the Pt dimer, the triplet state is energetically most favorable, followed by the singlet and the quintet state, respectively, in agreement with other DFT studies[85,86]. The results of the relative energy, E_{rel} (the energy relative to the lowest spin-state), binding energy and bond length for different spin multiplicities of Pt atom and dimer are shown in Table 1. The spin multiplicities have a large effect on the binding energy of the Pt dimer, but the bond length remains relatively constant.

Table 1 Relative energy, E_{rel}, (the energy related to the lowest spin-state), binding energy (E_b), and bond lengths for the Pt atom and dimer, for different spin multiplicities (2S + 1).

M	2S+1	E_{rel}(eV)	E_b(eV)	d_{Pt-Pt}(Å)
Pt	1	0.12	-	-
	3	0.00	-	-
	5	5.40	-	-
Pt_2	1	0.58	-2.84	2.35
	3	0.00	-3.42	2.36
	5	0.99	-2.42	2.38

There are several theoretical[86–93] and experimental[94–97] investigations of platinum clusters. For the triplet state of the Pt dimer, our calculated bond length is 2.36 Å which is in excellent agreement with the experimental bond length of 2.33 Å[97] and within the range of 2.33-2.45 Å, reported by using different computational methods[86,88–91]. The calculated binding energy for Pt dimer is -3.42 eV, in excellent agreement with experimental values of 3.64 $\pm$0.16[94] and 3.14 $\pm$0.02 eV[95].

Adopting a valence bond approach, the bonding in transition-metal dimers can be described as a multiple bond formed between two atoms in a $d^n s$ state. As established[98,99], the metal-metal bonding is dominated by delocalized valence $s-s$ interactions for the Pt dimer, and the valence d electrons mostly remain localized on each metal center and only weakly couple in the low-lying states. This contribution is, however, non-negligible and can not be simulated by a one-electron pseudopotential[100].

For the triplet state of the Pt dimer the two singly occupied molecular orbitals (SOMOs) are actually not the highest occupied orbitals, which instead is a doubly occupied orbital. Therefore, the highest occupied molecular orbital (HOMO) and the lowest unoccupied molecular orbital (LUMO) of the triplet Pt dimer (see Table 2) mainly consists of localized d orbitals, while the σ and σ^* orbitals, that contain large s character, are much lower and higher in energy, respectively. According to the compositions of the HOMO and LUMO, we can see that there exists hybridization among Pt_{6s}, Pt_{6p}, and Pt_{5d} atomic orbitals in the formation of the Pt dimer and s-d hybridization does play an important role in maximizing the overlap between molecular orbitals in dimer while the s-p hybridization is of negligible importance. Based on this bond picture, we can discuss the interaction between the PAH and Pt atoms in the next sections.

Table 2 The compositions of the HOMO and LUMO molecular orbitals for the Pt dimer at the triplet state. The numbers are the coefficients of atomic orbital in the molecular orbitals.

HOMO	LUMO
0.8703 5d	0.9774 5d
0.1572 6s	0.0000 6s
-0.0178 6p	0.0182 6p

3.2 PAH model

Some oligoacenes have an open-shell singlet ground state[101,102], and we therefore investigated the electronic ground state of our PAH model. By time-dependent DFT[103], the first singlet-singlet excitation energy was calculated to 1.79 eV and the first singlet-triplet excitation energy to 1.14 eV. We also did a geometry optimization of the triplet state of the PAH (assuming that

the triplet state would be just above the open-shell singlet state if the singlet diradical is the ground state) and found that the triplet state is 1.0 eV higher than the closed-shell singlet state. Our calculations thus confirm that we have a closed-shell PAH system in our example. Still, the ground-state needs to be verified for each PAH system studied.

3.3 Pt atom on the PAH surface

A single Pt atom has been placed in a hollow (surrounded by six carbon atoms), top (above a carbon atom), and bridge (between two neighboring carbon atoms) positions of the PAH molecule (see Fig. 1). There are several possibilities and initially we looked at many more adsorption configurations, but we only present three positions as representative of bridge, top and hollow sites.

After adsorption of the single Pt atom, the PAH molecule becomes bent in agreement with previous studies [14,104]. Chi et al. [104] investigated the adsorption of a single Pt atom on bent graphene surfaces with different curvatures, and the adsorption energies showed that the curvature of the graphene surface strengthened the Pt atom adsorption on graphene. Our work is consistent with these results.

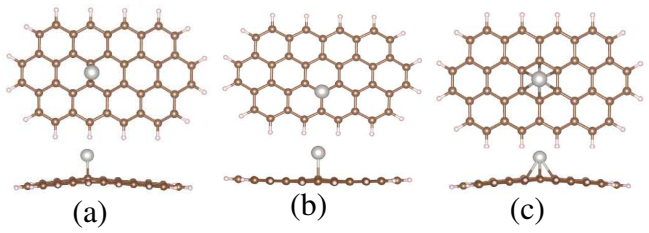

Fig. 1 Stable configurations for the Pt atom adsorption on the $C_{40}H_{16}$ molecule. Gray, brown and pink circles indicate Pt, C, and H atoms, respectively. a, b, c are bridge, top and hollow sites, respectively.

In agreement with recent calculations the bridge site is found to be energetically most favorable [26,28,30,33,47], followed by the top and hollow sites, respectively. Yazyev and Pasquarello [26] examined trends across the transition-metal series. They found adsorption in a hollow site to be favored for most metals, with the exception of Ir, Pd, and Pt where the bridge site is favored. Dai et al. [28] also found bridge adsorption to be favored for Pt clusters on graphene surface. Jiménez-Halla et al. found for the interaction of $Cr(CO)_3$ on a PAH fragment that the bridge and top sites are transition states between two hollow sites [105,106].

The binding energy and the Pt-C bond distances at all binding sites and all spin states are summarized in Table 3. The isolated PAH molecule has a calculated C-C distance of 1.43 Å. Upon adsorption, the C-C distances at the adsorption sites increase significantly, indicating a significant filling of the π^* MOs by back-donation from the Pt_{5d} orbitals. The most notable increase is found for the C-C bond in the bridge site (Fig. 1a) of 1.46 Å. The increase of the C-C bond length for the hollow site is not considerable, indicating less back-donation into the π^* MOs. The Pt-C distances for the top site (Fig. 1b) are shorter, but energetically, the bridge sites are more favorable. At the bridge site, two of the p_z orbitals of the PAH surface are well aligned for overlap with the Pt_{5d} orbitals, leading to a strong Pt-C bond and a high adsorption energy.

For a single Pt atom on the PAH surface, we find that the closed-shell ($5d^{10}6s^0$) singlet state is the electronic ground state. This is in agreement with a recent study where it is found that the closed-shell singlet state is the ground-state of the Pt-benzene complex [74]. The singlet-triplet energy separations for this complex are 0.68, 0.99 and 0.73 eV for bridge, top and hollow site, respectively, as given in Table 3, so the singlet state is considerably more stable for all three binding sites. The quintet states are higher in energy.

Table 3 Results for Pt adsorption on $C_{40}H_{16}$ with structures according to Fig. 1. all energies are in eV, distances are in Å.

Adsorption site	2s+1	$E_{ads.}$	d_{Pt-C}
a-Bridge	1	-2.17	2.08
	3	-1.49	2.08
	5	-0.12	2.25
b-Top	1	-2.15	2.01
	3	-1.16	2.02
	5	-0.09	2.16
c-Hollow	1	-1.74	2.39
	3	-1.01	2.39
	5	0.03	2.47

The transition (from triplet to singlet) results from σ-donation from the π orbitals of PAH to the vacant 6*s* atomic orbital of platinum atom and π-back donation of electron density from the 5*d* orbitals of Pt atom, which now become completely filled, to the π^* orbitals of the double bond of the PAH molecule. These donation and back donation of electron density tend to reduce the carbon-carbon bond order, leading to an elongated C-C distance. This phenomenon is illustrated in the density plots of the molecular orbitals of the Pt/PAH complex in Fig. 2. The forward and backward charge transfer between the Pt atom and the PAH is identified in the Figs. 2b and 2c). Consequently, the interaction between the Pt atom and the PAH molecule can be characterized according to the Dewar-Chatt-Duncanson model[107–109].

Hirshfeld atomic charges[81] of the isolated PAH molecule are shown in Fig. 3. The atomic charges will be altered if a Pt atom is adsorbed on the PAH molecule. In the Table 4 the Pt charge and the atomic charge for the carbon atom at the adsorption site is shown. The most significant charge transfer occur on the Pt atoms which become positive upon adsorption and reveals electron transfer from the Pt atom to the PAH molecule, in agreement with previous studies[28,30]. Upon adsorption, the charge transfer is the smallest for the hollow site and the largest for the top site. By comparing the Pt-C bond distance and the charge transfer on different sites, the magnitude of the charge transfer decreases with Pt-C bond elongation. This is consistent with a recent charge-transfer model based on a modified electronegativity equalization scheme[110], where the amount of charge-transfer depends strongly on the bond length.

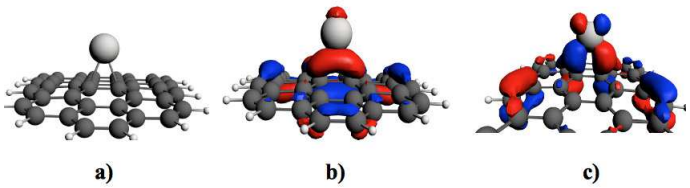

Fig. 2 a) Structure of the Pt/PAH complex for the bridge site. b) and c) are the density plots of the molecular orbitals of the Pt atom on the bridge site. b) shows the donation process from the π orbitals of the PAH molecule to a 6*s* orbitals of the Pt atom. c) shows the back-donation process from the 5*d* orbitals of the Pt atom to the π^* orbitals of the PAH surface. The two isosurfaces correspond to a density value of 0.03 a.u.. Light and dark gray circles indicate Pt and C atoms, respectively. Small light gray circles indicates H atoms.

Table 4 Hirshfeld charges (au.) before and after adsorption of the Pt atom on the PAH surface. The charge of C is the average value of the charges at the adsorption sites.

Atom	before ads.	after ads. at bridge site	after ads. at top site	after ads. at hollow site
Pt	0.000	0.191	0.199	0.166
C	0.003	-0.047	-0.051	-0.011

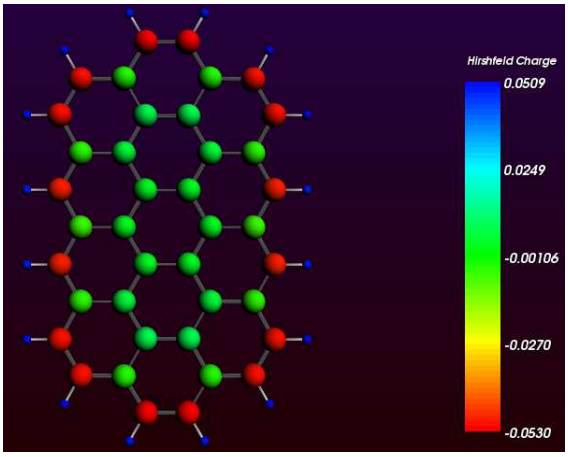

Fig. 3 The Hirshfeld atomic charges distributed on the $C_{40}H_{16}$ surface.

3.4 Pt dimer on the PAH surface

For adsorption of the Pt dimer on the PAH surface, there are several possibilities and initially, as for the Pt/PAH system, we looked at many more adsorption configurations, but we only present some configurations as representative for the bridge, top and hollow sites, respectively. The distortion of the PAH and the Pt dimer upon adsorption at different adsorption sites are summarized in Fig. 4 and Table 5.

For adsorption of two separated Pt atoms on two bridge sites (Fig. 4a), E_{ads} is larger than twice of E_{ads} of the single Pt atom by 0.08 eV, which is due to weak interactions between the neighbouring Pt atoms on the surface. The adsorption energy of the Pt dimer on two neighbouring bridge site (Fig. 4b) is -5.05 eV. This larger adsorption energy, by 0.63 eV, is a result of the Pt-Pt bond, indicating that aggregation of Pt atoms on the PAH surface is

favorable, in agreement with observations by STM[111].
In addition, because of a strong edge interaction and relatively short Pt-C bond distance, the dimer close to the edge in Fig. 4c is slightly more stable than the dimer in Fig. 4b. This interaction leads to that, the C-H bonds at the edge is tilted out of the PAH plane and cause a rehybridization of the carbon atom, from sp^2 to sp^3-like. This is in agreement with previous studies and the activity of carbon atoms declines from edge to the center[112].
Next we examined the interaction between the Pt dimer and the PAH surface for top (see Figs. 4d-f) and hollow sites (see Figs. 4g and h), respectively. The adsorption energy of the Pt dimer on the two neighboring top (Fig. 4d) and hollow (Fig. 4h) sites are 4.82 and 4.62 eV, respectively. These values are larger than the adsorption energy of two separated Pt atoms at the corresponding positions on the PAH surface (see Figs. 4e-g and Table 5), which indicates that aggregation of Pt atoms at these positions are also favorable. The strong edge interaction of the Pt atoms in Fig. 4f leads to a higher adsorption energy in respect to Fig. 4e, by 0.51 eV. In Fig. 4f, the C-H bond at the adsorption sites is again tilted out from the PAH plane for a better overlap of the molecular orbitals and again it causes a rehybridization of the carbon atom from sp^2 to sp^3-like.
In agreement with recent ab initio calculations the bridge site is found to be energetically most favorable[30,33], followed by the top and hollow positions. Comparing the three adsorption sites, the Pt-C distance increases with the coordination of the Pt atom, from the top over the bridge to the hollow site.

In addition, we also placed the Pt dimer in an upright position on the PAH surface on the three adsoption sites, and optimized the structures (see Fig. 5). In this configuration, the hollow site is energetically most favorable, followed by the bridge and top sites, respectively, as seen in Table 6.
The interfacial interaction energy, E_{int}, which measures the interaction energy of Pt dimer with the PAH surface (see Tables 5 and 6), is smaller than the interaction energy of Pt atom on the surface (see Table 3). Therefore the binding of a single Pt atom to the surface is stronger than the binding of the Pt dimer to the surface. Hence the Pt-C bond length in the Pt/PAH complex is mostly shorter than the corresponding bond length in the Pt_2/PAH complex. The interfacial interaction for the up-

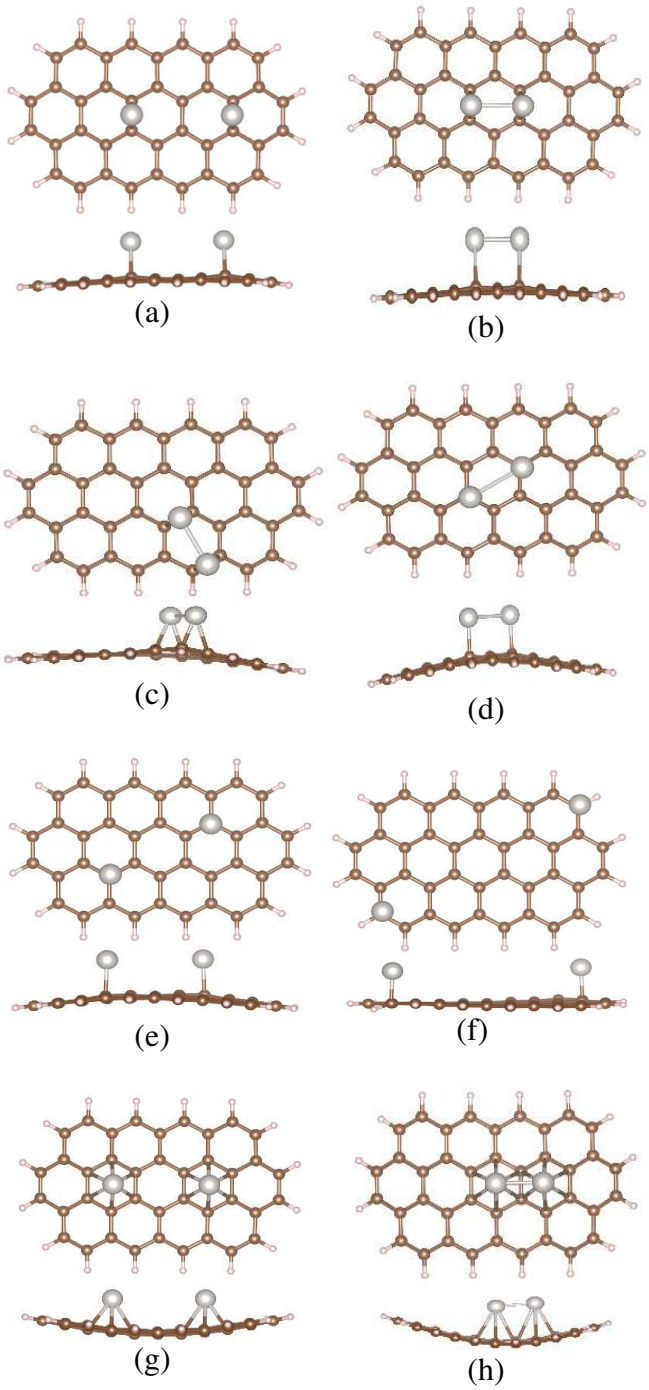

Fig. 4 Stable configurations for the Pt dimer (parallel adsorption) and two Pt atoms on $C_{40}H_{16}$ molecule. Gray, brown and pink circles indicate Pt, C, and H atoms, respectively. *a*, *b* and *c* are bridge sites, *d*, *e* and *f* are top sites and *g* and *h* are hollow sites.

Table 5 Results for Pt dimer adsorption on $C_{40}H_{16}$ with structures according to Fig. 4 . All energies are in eV, distances are in Å.

Ads. site	2s+1	E_{ads}	E_{int}	d_{Pt-Pt}	d_{Pt-C}
a-Bridge	1	-4.42	-	-	2.08
	3	-3.71	-	-	2.08
	5	-3.18	-	-	2.08
b-Bridge	1	-4.57	-1.16	2.56	2.19
	3	-5.05	-1.61	2.56	2.18
	5	-4.24	-0.83	2.56	2.19
c-Bridge	1	-4.66	-1.25	2.57	2.02
	3	-5.12	-1.70	2.57	2.05
	5	-4.45	-1.03	2.57	2.05
d-Top	1	-4.43	-1.01	2.82	2.09
	3	-4.82	-1.40	2.82	2.09
	5	-3.88	-0.46	2.82	2.09
e-Top	1	-4.19	-	-	2.02
	3	-3.49	-	-	2.06
	5	-2.58	-	-	2.06
f-Top	1	-4.70	-	-	2.03
	3	-4.61	-	-	2.02
	5	-2.91	-	-	2.02
g-Hollow	1	-4.01	-	-	2.41
	3	-3.41	-	-	2.42
	5	-2.69	-	-	2.42
h-Hollow	1	-4.03	-0.61	2.39	3.34
	3	-4.62	-1.20	2.40	3.34
	5	-3.92	-0.51	2.40	3.34

right configuration is more attractive than for the parallel configuration, and the highest interfacial interaction energy was found on the hollow site, for the upright configuration. The adsorption energy of the Pt dimer on the upright configuration is more stable than the parallel configuration due to the energy penalty for a Pt-Pt bond elongation in the parallel configuration.

The SSB-D functional predicts a bond length of 2.36 Å for the isolated Pt dimer. The experimental value of d_{Pt-Pt} in an STM observation on HOPG is 2.46 Å[38], which is longer than the bond length of the isolated dimer, due to surface interaction. The bond length of the Pt dimer on the bridge site is 2.56 and 2.38 Å, in

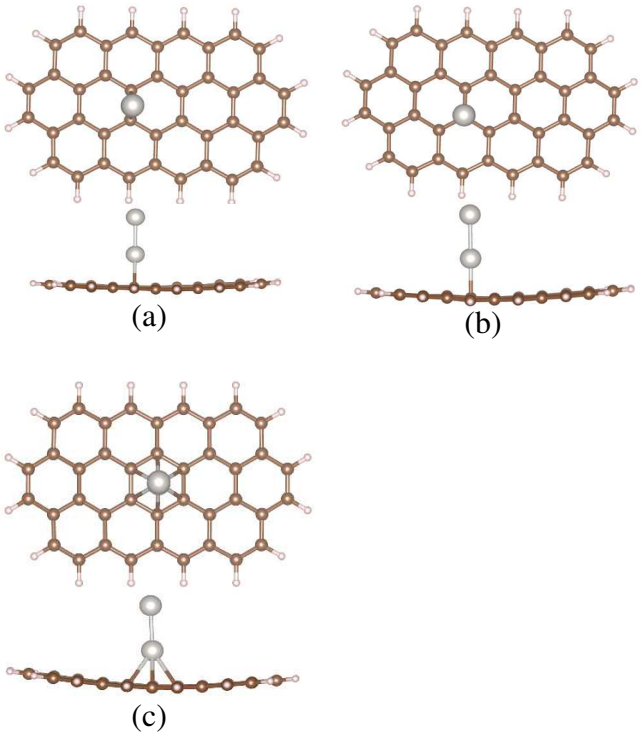

Fig. 5 Stable configurations for the Pt dimer (upright adsorption) on the $C_{40}H_{16}$ molecule. Gray, brown and pink circles indicate Pt, C and H atoms, respectively. *a*, *b* and *c* are bridge, top and hollow sites,respectively.

Table 6 Results for Pt dimer adsorption on $C_{40}H_{16}$ with structures according to Fig. 5. All energies are in eV, distances are in Å.

Ads. site	2s+1	E_{ads}	E_{int}	d_{Pt-Pt}	d_{Pt-C}
a-Bridge	1	-4.27	-0.85	2.38	2.27
	3	-4.92	-1.51	2.38	2.26
	5	-4.03	-0.61	2.38	2.26
b-Top	1	-4.27	-0.85	2.39	2.13
	3	-4.45	-1.04	2.39	2.13
	5	-4.09	-0.68	2.37	2.18
c-Hollow	1	-4.50	-1.08	2.37	2.35
	3	-5.06	-1.64	2.38	2.35
	5	-3.95	-0.53	2.38	2.35

the parallel and upright configuration, respectively. The experimental value is somewhere in between these two configurations. For both cases, due to the influence of

the PAH surface, the Pt-Pt distances are longer than the isolated Pt dimer, but the upright system attain a value much closer to the Pt-Pt distances for the isolated dimer. For adsorption of the parallel dimers (Table 5 and Fig. 4), the Pt-Pt bond distance has to be slightly elongated to fit the binding sites on the PAH, which gives a slight destabilization of the Pt-Pt interaction. This change in the Pt-Pt bond length has an important role in the enhancement of its catalytic activity[35].

In contrast to the Pt/PAH system, the interaction of Pt dimer with the PAH surface is not accompanied by a change of spin state, and the most stable spin state is still a triplet state. This confirms that the Pt-C interaction is weaker than the Pt-Pt interaction. Therefore for the Pt dimer on the surface, the triplet state is the most stable, but for the two separate Pt atom, the singlet state is the most stable followed by the triplet state, as for the single Pt atom on the surface (see Tables 5 and 6).

Concerning the nature of the bonding in the Pt_2/PAH complex, the overlap of the $6s-6s$ metal orbitals are mainly responsible for formation of a σ-bond between the Pt atoms on the PAH surface (see Figs. 6a and 7a). Analysis of molecular orbitals shows that, as for the Pt/PAH complex, an overlap of the $5d$ orbital of the Pt dimer with the π molecular orbitals of the PAH molecule are responsible for the stability of the Pt dimer on the PAH surface. The density plots of the molecular orbitals of the Pt dimer on the bridge site at parallel and upright configuration are shown in Fig. 6 and Fig. 7, respectively.

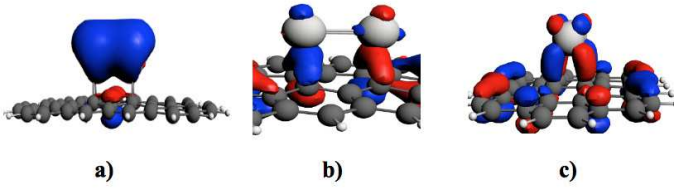

Fig. 6 The density plots of the molecular orbitals of the Pt dimer on the bridge site at parallel configuration. a) shows the overlap of the $6s-6s$ metal orbitals that mainly responsible for formation of Pt-Pt bond. b) shows the donation process from the π orbitals of the PAH molecule to a $6s-5d$ hybride orbitals of the Pt dimer. c) shows the back-donation process from the $5d$ orbitals of the Pt atom to the π^* orbitals of the PAH surface. The two isosurfaces correspond to a density value of 0.03 a.u.. Color coding as in Fig. 2.

Figs. 6a and 7a, show the molecular orbitals that mainly constitute the Pt-Pt bonding on the PAH surface. Figs. 6b and 7b show the donation process from the π orbitals of the PAH molecule to a $6s-5d$ hybride orbitals of the Pt dimer and Fig. 6c and 7c, show the back-donation process from the $5d$ orbitals of Pt atom to the π^* orbitals of PAH surface. The donation and backdonation charge density between the Pt atoms and the PAH molecule is illustrated in these figures. Again, the interaction between the Pt atom and dimer with the PAH molecule can be characterized by the Dewar-Chatt-Duncanson model[107–109].

Hirshfeld atomic charges for the carbon atoms of the PAH molecule and for the platinum atoms of the dimer at the adsorption sites, before and after adsorption, are listed in Table 7. A positive charge on the Pt atom reveals that there is an electron transfer from the Pt atoms to the PAH surface, and this is consistent with the adsorption of a single Pt atom on the surface. For the upright adsorption of the Pt dimer on the surface, however, a negative charge is found on the upper Pt atom of the Pt dimer. In general, the C and Pt atoms have very similar electronegativities so the sign of the atomic charges may be reversed by modifying the surroundings[47]. In contrast to the parallel configuration, the charge transfer at the hollow site is larger than for the bridge and top sites for the upright configuration (see Table 7).

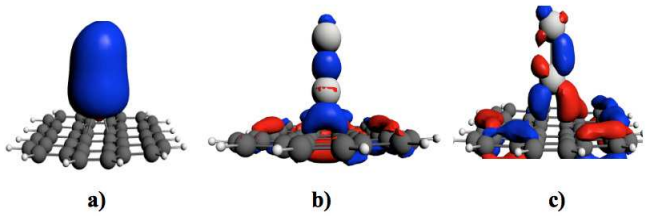

Fig. 7 The density plots of the molecular orbitals of the Pt dimer on the bridge site at upright configuration. a) shows the overlap of the $6s-6s$ metal orbitals that mainly responsible for formation of Pt-Pt bond. b) shows the donation process from the π orbitals of the PAH molecule to a $6s-5d$ hybride orbitals of the Pt dimer. c) shows the back-donation process from the $5d$ orbitals of the Pt atom to the π^* orbitals of the PAH surface. The two isosurfaces correspond to a density value of 0.03 a.u.. Color coding as in Fig. 2.

Table 7 Hirshfeld atomic charges (au.) before and after adsorption of the Pt dimer on the PAH surface. For the parallel adsorption, the bridge, top and hollow are refer to the Figs. 4b, 4d and 4h respectively. For the upright adsorption, the bridge, top and hollow are refer to the Figs. 5a, 5b and 5c respectively. The values in parentheses are the atomic charges related to upper Pt atom of the dimer in the upright adsorption. The charge of C are calculated as in Table 4.

Conf.	Atom	before ads.	after ads. bridge	after ads. top	after ads. hollow
Parallel	Pt	0.000	0.14	0.12	0.06
	C	0.003	-0.040	-0.052	-0.021
Upright	Pt	0.000	0.14(-0.12)	0.14(-0.12)	0.19(-0.17)
	C	0.003	-0.046	-0.060	-0.026

4 Conclusions

A detailed density functional study of the Pt atom and dimer adsorption on a PAH molecule is presented. The preferred adsorption sites were found to be the bridge site for the Pt atom and parallel dimer and hollow site for the upright dimer configuration, respectively. Upon adsorption of a single Pt atom, the electronic state of the Pt atom is found to change from the triplet ground state ($5d^9 6s^1$), to the closed-shell singlet state ($5d^{10} 6s^0$), which will affect the catalytic activity of the Pt atom as compared to the open-shell triplet state. In contrast, the adsorption of the Pt dimer is not accompanied by a change in spin state, and the most stable electronic state is still the triplet state. The molecular orbital analysis shows an overlap of the $5d$ orbital of the Pt atom and dimer with the π molecular orbitals of the PAH molecule, which are responsible for the stability of the Pt atom and dimer on the PAH surface. The overlap of the $6s - 6s$ Pt orbitals are mainly responsible for formation of a Pt-Pt σ-bond. A forward and backward charge transfer between the Pt atom and the PAH was identified in the bonding. Consequently, the interaction between the Pt atom and the PAH molecule can be characterized by the Dewar-Chatt-Duncanson model. While the atomic charge on the Pt atoms and dimers (in parallel configuration) are positive, a negative atomic charge is found on the upper Pt atom for the upright configuration. The sign of the atomic charge will have a large effect on the catalytic activity and may be an explanation for different activity between a single layer of Pt atoms and Pt clusters on carbon surfaces. Comparing the Pt-C bond length and the charge transfer on different sites, the magnitude of the charge transfer decrease with bond elongation, indicating that the catalytic activity of the Pt atom and dimer can be changed by modifying its chemical surroundings.

The adsorption energy for the Pt dimer on the PAH surface is larger than for two individual Pt atoms on the surface, which indicates that aggregation of Pt atoms on the PAH surface is favorable. Analysis of the energetics indicate that the binding of the Pt dimer to PAH is relatively weak, whereas the binding between the Pt atoms forming the dimer is larger than in the isolated dimer. The adsorption energy is higher for the dimer than for the isolated Pt atoms, hence dimerization is predicted to be energetically favored, in agreement with observations by STM.

The results indicate that the Pt dimer on graphene could be an attractive catalyst system, where the properties can be tuned by manipulating the carbon electron density through defects, oxygen groups and doping .

5 Acknowledgment

This work is a part of an ISP project with financial support from the Norwegian Research Council. Computational time provided by the Notur project is acknowledged.

References

1 A. K. Geim and K. S. Novoselov, *Nature Materials*, 2007, **6**, 183–191.
2 M. I. Katsnelson, *Mat. Today*, 2007, **10**, 20–27.
3 K. S. Novoselov, A. K. Geim, S. V. Morozov, D. Jiang, Y. Zhang, S. V. Dubonos, I. V. Grigorieva, and A. A. Firsov, *Science*, 2004, **306**, 666–669.
4 M. F. El-Kady, V. Strong, S. Dubin, and R. Kaner, *Science*, 2012, **335**, 1326–1330.
5 M. S. Dresselhaus and G. Dresselhaus, *Adv. Phys.*, 1981, **30**, 139–326.
6 B. T. Kelly, *Physics of Graphite*, Applied Science, London, 1981.
7 X. Wang, L. Zhi, and K. Müllen, *Nano Lett.*, 2008, **8**, 323–327.
8 C. Lee, X. Wei, J. Kysar, and J. Hone, *Science*, 2008, **321**, 385–388.
9 G. Giovannetti, P. A. Khomyakov, G. Brocks, V. M. Karpan, J. V. D. Brink, and P. J. Kelly, *Phys. Rev. Lett.*, 2008, **101**, 026803–4.

10 K. T. Chan, J. B. Neaton, and M. L. Cohen, *Phys. Rev. B*, 2008, **77**, 235430–12.
11 C. Cao, M. Wu, J. Z. Jiang, and H. P. Cheng, *Phys. Rev. B*, 2010, **81**, 205424–9.
12 H. Sevinçli, M. Topsaka, E. Durgun, and S. Ciraci, *Phys. Rev. B*, 2008, **77**, 195434–7.
13 B. Uchoa, C.-Y. Lin, and A. H. C. Neto, *Phys. Rev. B*, 2008, **77**, 035420–5.
14 Y. Okamoto, *Chem. Phys. Lett.*, 2006, **420**, 382–386.
15 K. Okazaki-Maeda, S. Yamakawa, Y. Morikawa, T. Akita, S. Tanaka, S. Hyodo, and M. Kohyama, *J. Phys.: Conf. Ser.*, 2008, **100**, 072044–4.
16 S. Jayaraman and A. C. Hillier, *Meas. Sci. Technol*, 2005, **16**, 5–13.
17 S. Basri, S. Kamarudin, W. Daud, and Z. Yaakub, *Int. J. Hydrogen Energy*, 2010, **35**, 7957–7970.
18 C. K. Acharya, D. I. Sullivan, and C. H. Turner, *J. Phys. Chem. C*, 2008, **112**, 13607–13622.
19 M. Chen and D. Goodman, *Catal. Today*, 2006, **111**, 22–33.
20 T. Frelink, W. Visscher, and J. van Veen, *J. Electroanal. Chem.*, 1995, **382**, 65–72.
21 C. Prado-Burguete, A. Linares-Solano, F. Rodriguez-Reinoso, and C.-M. D. Lecea, *J. Catal.*, 1991, **128**, 397–404.
22 S. A. Lee, K. W. Park, J. H. Choi, B. K. Kwon, and Y. E. Sung, *J. Electrochem. Soc.*, 2002, **149**, 1299–1304.
23 S. Mukerjee and J. McBreen, *J. Electroanal. Chem.*, 1998, **448**, 163–171.
24 R. Narayanan and M. A. El-Sayed, *Nano Lett.*, 2004, **4**, 1343–1348.
25 S. Park, S. A. Wasileski, and M. J. Weaver, *J. Phys. Chem. B*, 2001, **105**, 9719–9725.
26 O. V. Yazyev and A. Pasquarello, *Phys. Rev. B*, 2010, **82**, 045407–5.
27 K. Kong, Y. Choi, B. Ryu, J. Lee, and H. Chang, *Mat. Sci. Eng. C*, 2006, **26**, 1207–1210.
28 X.-Q. Dai, Y.-N. Tang, J.-H. Zhao, and Y.-W. Dai, *J. Phys.: Condens. Matter*, 2010, **22**, 316005–6.
29 K. Okazaki-Maeda, Y. Morikawa, S. Tanaka, and M. Kohyama, *Mat. Res. Soc. Symp. Proc.*, 2005, **900**, 6–35.
30 K. Okazaki-Maeda, Y. Morikawa, S. Tanaka, and M. Kohyama, *Surf. Sci.*, 2010, **604**, 144–154.
31 I. Cabria, M. J. López, and J. A. Alonso, *Phys. Rev. B*, 2010, **81**, 035403–5.
32 A. Ishii, M. Yamamoto, H. Asano, and K. Fujiwara, *J. Phys.: Conf. Ser.*, 2008, **100**, 052087–4.
33 P. Blonski and J. Hafner, *J. Chem. Phys.*, 2011, **134**, 154705–12.
34 S. Lee, S. Han, J. Kang, J. Ryu, and H. Lee, *Surf. Sci.*, 2008, **602**, 1433–1439.
35 C. Sanz-Navarro, P.-O. Åstrand, D. Chen, M. Rønning, A. van Duin, T. Jacob, and W. Goddard, *J. Phys. Chem. A*, 2008, **112**, 1392–1402.
36 H.-Y. Cheng, Y.-A. Zhu, P.-O. Åstrand, D. Chen, P. Li, and X.-G. Zhou, *J. Phys. Chem. C*, 2013, **117**, 14261–14271.
37 I. Fampiou and A. Ramasubramanian, *J. Phys. Chem. C*, 2012, **116**, 6543–6555.
38 U. Müller, K. Sattler, J. Xhie, N. Venkateswaran, and G. Raina, *J. Vac. Sci. Technol. B*, 1991, **9**, 829–832.
39 U. Müller, K. Sattler, J. Xhie, N. Venkateswaran, and G. Raina, *Z. Phys. D: At. Mol. Clusters*, 1991, **19**, 319–321.
40 A. Howells, L. Hung, G. Chottiner, and D. Scherson, *Solid State Ionics*, 2002, **150**, 53–62.
41 P. Sony, P. Puschnig, D. Nabok, and C. Ambrosch-Draxl, *Phys. Rev. Lett.*, 2007, **99**, 176401–4.
42 N. Atodiresei, V. Caciuc, P. Lazić, and S. Blügel, *Phys. Rev. Lett.*, 2009, **102**, 136809–4.
43 M. Mura, A. Gulans, T. Thonhauserc, and L. Kantorovich, *Phys. Chem. Chem. Phys.*, 2010, **12**, 4759–4767.
44 J. Brede, N. Atodiresei, S. Kuck, P. Lazić, V. Caciuc, Y. Morikawa, G. Hoffmann, S. Blüge, and R. Wiesendanger, *Phys. Rev. Lett.*, 2010, **105**, 047204–4.
45 G. Mercurio, E. R. McNellis, I. Martin, S. Hagen, F. Leyssner, S. Soubatch, J. Meyer, M. Wolf, P. Tegeder, F. S. Tautz, and K. Reuter, *Phys. Rev. Lett.*, 2010, **104**, 036102–4.
46 D. Stradi, S. Barja, C. Diaz, M. Garnica, B. Borca, J. J. Hinarejos, D. Sánchez-Portal, M. Alcami, A. Arnau, A. L. V. de Parga, R. Miranda, and F. Martin, *Phys. Rev. Lett.*, 2011, **106**, 186102–4.
47 H.-Y. Cheng, P.-O. Åstrand, D. Chen, Y.-A. Zhu, X.-G. Zhou, and P. Li, *Chem. Phys. Lett.*, 2013, **575**, 76–80.
48 J. P. Perdew, K. Burke, and M. Ernzerhof, *Phys. Rev. Lett.*, 1996, **77**, 3865–3868.
49 A. Bilić, J. R. Reimers, N. S. Hush, R. C. Hoft, and M. J. Ford, *J. Chem. Theory Comput.*, 2006, **2**, 1093–1105.
50 S. Grimme, *J. Comput. Chem.*, 2004, **25**, 1463–1473.
51 S. Grimme, *J. Comput. Chem.*, 2006, **27**, 1787–1799.
52 P. Bloński and J. Hafner, *J. Chem. Phys.*, 2012, **136**, 074701–11.
53 M. Swart, M. Solà, and F. M. Bickelhaupt, *J. Comput. Meth. Sci. Engin.*, 2009, **9**, 69–77.
54 M. Swart, M. Solà, and F. M. Bickelhaupt, *J. Chem. Phys.*, 2009, **131**, 094103–9.
55 K. S. Pitzer, *Acc. Chem. Res.*, 1979, **12**, 271–276.
56 P. Pyykko and J. P. Desclaux, *Acc. Chem. Res.*, 1979, **12**, 276–281.
57 P. Pyykko, *Chem. Rev.*, 1988, **88**, 563–594.
58 P. A. Christiansen, W. C. Ermler, and K. S. Pitzer, *Annu. Rev. Phys. Chem.*, 1985, **36**, 407–432.
59 P. A. M. Dirac, Clarendon Press: Oxford, U.K., 1958; chapter XI; 4th ed.
60 M. Douglas and N. M. Kroll, *Ann. Phys.*, 1974, **82**, 89–155.
61 B. A. Hess, *Phys. Rev. A*, 1986, **33**, 3742–3748.
62 A. Wolf, M. Reiher, and B. A. Hess, *J. Chem. Phys.*, 2002, **117**, 9215–9226.
63 E. van Lenthe, A. Ehlers, and E. Baerends, *J. Chem. Phys.*, 1999, **110**, 8943–8953.
64 E. v. Lenthe, E. J. Baerends, and J. G. Snijders, *J. Chem. Phys.*, 1993, **99**, 4597–4610.
65 E. v. Lenthe, E. J. Baerends, and J. G. Snijders, *J. Chem. Phys.*, 1994, **101**, 9783–9792.

66 E. van Lenthe, J. Snijders, and E. Baerends, *J. Chem. Phys.*, 1996, **105**, 6505–6516.

67 E. van Lenthe, R. van Leeuwen, E. J. Baerends, and J. G. Snijders, *Int. J. Quant. Chem.*, 1996, **57**, 281–293.

68 J. L. Heully, I. Lindgren, E. Lindroth, S. Lundqvist, and A. M. Martensson-Pendrill, *J. Phys. B: At. Mol. Phys.*, 1986, **19**, 2799–2815.

69 D. A. Pantazis and F. Neese, *WIREs Comput. Mol. Sci.*, 2014, **4**, 363–374.

70 P. J. Hay and W. R. Wadt, *J. Chem. Phys.*, 1985, **82**, 299–310.

71 W. J. Stevens, H. Basch, and M. Krauss, *J. Chem. Phys.*, 1984, **81**, 6026–6033.

72 T. R. Cundari and W. J. Stevens, *J. Chem. Phys.*, 1993, **98**, 5555–5565.

73 A. N. Rudenko, F. J. Keil, M. I. Katsnelson, and A. I. Lichtenstein, *Phys. Rev. B*, 2012, **86**, 075422–11.

74 J. Granatier, M. Dubecky, P. Lazar, M. Otyepka, and P. Hobza, *J. Chem. Theory Comput.*, 2013, **9**, 1461–1468.

75 G. te Velde, F. M. Bickelhaupt, S. J. A. van Gisbergen, C. F. Guerra, E. J. Baerends, J. G. Snijders, and T. Ziegler, *J. Comput. Chem.*, 2001, **22**, 931–967.

76 C. F. Guerra, J. G. Snijders, G. te Velde, and E. J. Baerends, *Theor. Chem. Acc.*, 1998, **99**, 391–403.

77 E. V. Lenthe and E. J. Baerends, *J. Comput. Chem.*, 2003, **24**, 1142–1156.

78 M. Güell, J. M. Luis, M. Solá, and M. Swart, *J. Phys. Chem. A*, 2008, **112**, 6384–6391.

79 M. Swart, *Chem. Commun.*, 2013, **49**, 6650–6652.

80 M. Costas and J. N. Harvey, *Nat. Chem.*, 2013, **5**, 7–9.

81 F. L. Hirshfeld, *Theor. Chim. Acta*, 1977, **44**, 129–138.

82 K. B. Wiberg and P. R. Rablen, *J. Comput. Chem.*, 1993, **14**, 1504–1518.

83 K. Momma and F. Izumi, *J. Appl. Cryst.*, 2008, **41**, 653–658.

84 C. E. Moore, *Atomic Energy Levels*, Natl Bur. Stand. (U.S.) Circ., 1971.

85 H. Grönbeck and W. Andreoni, *Chem. Phys.*, 2000, **262**, 1–14.

86 K. Bhattacharyya and C. Majumder, *Chem. Phys. Lett.*, 2007, **446**, 374–379.

87 Q. Cui, D. G. Musaev, and K. Morokuma, *J. Chem. Phys.*, 1998, **108**, 8418–8428.

88 K. Balasubramanian, *J. Chem. Phys.*, 1987, **87**, 6573–6578.

89 S. H. Yang, D. A. Drabold, J. B. Adams, P. Ordejon, and K. Glassford, *J. Phys.: Condens. Matter*, 1997, **9**, L39–L45.

90 T. Li and P. B. Balbuena, *J. Phys. Chem. B*, 2001, **105**, 9943–9952.

91 A. Sebetci, *Chem. Phys.*, 2006, **331**, 9–18.

92 W. Q. Tian, M. Ge, B. R. Sahu, D. Wang, T. Yamada, and S. Mashiko, *J. Phys. Chem. A*, 2004, **108**, 3806–3812.

93 M. N. Huda, M. K. Niranjan, B. R. Sahu, and L. Kleinman, *Phys. Rev. A*, 2006, **73**, 053201–5.

94 S. K. Gupta, B. M. Nappi, and K. A. Gingerich, *Inorg. Chem.*, 1981, **20**, 966–969.

95 S. Taylor, G. W. Lemire, Y. M. Hamrick, Z. Fu, and M. D. Morse, *J. Chem. Phys.*, 1988, **89**, 5517–5523.

96 A. Grushow and K. M. Ervina, *J. Chem. Phys.*, 1997, **106**, 9580–9593.

97 M. B. Airola and M. D. Morse, *J. Chem. Phys.*, 2002, **116**, 1313–1317.

98 H. Wang and E. Carter, *J. Phys. Chem.*, 1992, **96**, 1197–1204.

99 W.-X. Xu, K. D. Schierbaum, and W. Goepel, *Int. J. Quant. Chem.*, 1997, **62**, 427–436.

100 S. Zurita, J. Rubio, F. Illas, and J. C. Barthelat, *J. Chem. Phys.*, 1996, **104**, 8500–8506.

101 M. Bendikov, H. M. Duong, K. Starkey, K. N. Houk, E. A. Carter, and F. Wudl, *J. Am. Chem. Soc.*, 2004, **126**, 7416–7417.

102 J. Poater, J. M. Bofill, P. Alemany, and M. Solá, *J. Phys. Chem. A*, 2005, **109**, 10629–10632.

103 E. K. U. Gross, J. F. Dobson, and Petersilka, Springer: Heidelberg, 1996.

104 D. Chi, N. Cuong, N. Tuan, Y. Kim, H. Bao, T. Mitani, T. Ozaki, and H. Nagao, *Chem. Phys. Lett.*, 2006, **432**, 213–217.

105 J. O. C. Jiménez-Halla, J. Robles, and M. Solá, *J. Phys. Chem. A*, 2008, **112**, 1202–1213.

106 J. O. C. Jiménez-Halla, J. Robles, and M. Solá, *Organometallics*, 2008, **27**, 5230–5240.

107 M. J. S. Dewar, *Bull. Soc. Chim. Fr.*, 1951, **18**, C79.

108 J. Chatt and L. A. Duncanson, *J. Chem. Soc.*, 1953, pp. 2939–2947.

109 D. M. P. Mingos, *J. Organomet. Chem.*, 2001, **635**, 1–8.

110 H. S. Smalø, P.-O. Åstrand, and L. Jensen, *J. Chem. Phys.*, 2009, **131**, 044101–19.

111 Z. Zhou, F. Gao, and D. W. Goodman, *Surf. Sci.*, 2010, **604**, L31–L38.

112 C. Zhou, J. Hu, Y. Tian, Q.-Y. Zhao, L. Miu, and J.-J. Jiang, *J. At. Mol. Sci.*, 2012, **3**, 270–278.